IEEE Access
Multidisciplinary ⋮ Rapid Review ⋮ Open Access Journal

Received 21 May 2024, accepted 15 June 2024, date of publication 27 June 2024, date of current version 1 August 2024.

Digital Object Identifier 10.1109/ACCESS.2024.3420088

RESEARCH ARTICLE

Low Frequency Oscillation Suppression of Three-Phase Four-Wire Inverter Based on CFM-OSG Phase-Locked Loop

GUOXUAN CUI[1], YANWEN WANG[1], AND LIYA LIU[2]
[1]School of Mechanical and Electrical Engineering, China University of Mining and Technology, Beijing 100083, China
[2]Beijing Bowang Technology Company Ltd., Beijing 100070, China

Corresponding author: Guoxuan Cui (cuiguoxuan2023@126.com)

This research was funded by the National Natural Science Foundation of China: Research on key technologies of mine asymmetric magnetic coupling resonant wireless power transmission-No. 52074305.

ABSTRACT To handle the low frequency oscillations of the three-phase four-wire inverter grid-connected system caused by small phase-locked range, slow locking speed and large steady-state error of the traditional phase-locked loop, an improved phase-locked loop is proposed to suppress low frequency oscillation. Firstly, the paper established a sequence impedance model of three-phase four-wire inverter, and analyzed the impact of the phase-locked loop on low frequency stability in a weak power grid and the mechanism of low frequency oscillations. Secondly, based on the cross-coupling method of the Complex Filter Matrix (CFM)-Orthogonal Signal Generator (OSG), the paper combined a first-order complex filter with a positive-negative sequence voltage component relationship matrix to form an improved phase-locked loop. The improved phase-locked loop is used to reshape the positive sequence, negative sequence and zero sequence impedance of the inverter, which not only increased the impedance amplitude of the inverter system, but also realized low frequency oscillations suppression. Finally, applying the simulation and experimentation, the paper verified the validity of the established sequence impedance and the effectiveness of the proposed improved phase-locked loop to suppress low frequency oscillation in the three-phase four-wire weak power grid.

INDEX TERMS Weak grid systems, three-phase four-wire system, sequential impedance modeling, complex filter matrixes, orthogonal signal generator.

I. INTRODUCTION

With the continuous and prosperous development of the digital age and the guidance of the goals of ''Carbon Neutrality'' and ''Carbon Peaking'', new energy power generation systems taking high-efficiency semiconductors as power equipment are increasingly emphasized by the world. Most of these new energy power plants are far from the load center, long-distance electric transmission lines are necessary when connecting to the grid, and the impedance of the new energy power generation system is relatively small. Therefore, new energy grid connection inverters, electric transmission lines, and output filters constitute the weak current grid system. Standing from the perspective of the grid connection point, the impedance of the power system is relatively high, with Short Circuit Ratio (SCR) commonly less than 3, which is likely to cause system oscillations [1], [2]. In recent years, multiple forms of oscillation problems related to new energy units occurred to varying degrees around the world. For example, the oscillations caused by the interaction between electric transmission lines and inverters during the grid connection process of the Borwin1 wind power plant booster station in Germany [3], [4], and oscillations caused by the interaction between electric transmission lines and power electronic equipment during the operation of the Chongqing Hubei Interconnection Project in China [5], [6]. The high occurrence of oscillations not only threats the safe operation of power electronic equipment, but also reduces the stability and reliability of the entire power system operation. When oscillations occurs, it will produce power grid harmonics and

The associate editor coordinating the review of this manuscript and approving it for publication was Ha Nguyen.

cause power grid distortion. The total harmonic distortion (THD) is usually used to characterize the distortion degree of the waveform. The larger the THD value, the more serious the waveform distortion and the richer the harmonics. The smaller the THD value, the smaller the waveform distortion and the smaller the harmonic component.

Currently, there are two control strategies of grid connection inverters orienting to the systems with low frequency oscillations [7], [8], [9], [10], [11], [12], [13], [14], [15]: 1) Single current loop control; 2) The dual loop control of the DC voltage outer loop and the AC current inner loop [9], [16]. The above two control strategies basically use phase-locked loops to obtain the phase of the power grid, which determines that the design of the phase-locked loop is of great significance to the grid-connected system, and unreasonable design can lead to low frequency oscillations of the grid-connected system [17], [18], [19]. Therefore, analyzing the mechanism of low frequency oscillation and the impact of phase-locked loops on low frequency oscillation is of important theoretical and practical significance, which is beneficial for improving the impedance characteristics of grid connection inverters and achieving stable operation of larger-scale new energy grid connection systems.

The key to the accurate phase locking of the phase-locked loop is the extraction of the fundamental positive sequence signal. At present, the traditional phase-locked loop uses a low-pass filter for filtering on the synchronous coordinate dq axis, or directly limits the bandwidth of the PI controller for harmonic suppression. This method reduces the equivalent bandwidth of the system and reduces the dynamic response speed of the system. In the past two years, orthogonal signal generator (OSG) based on symmetrical component method has gradually become a research hotspot. The earliest and simplest OSG is based on the method of transmission delay [20]. When the frequency satisfies the condition, the PLL can output the correct result, but when the frequency fluctuates, the output signal is non-orthogonal. In [21] and [22], the method of constructing orthogonal components based on the delay of four frequency division periods is proposed, but the fixed sampling period cannot achieve accurate delay.

References [23] proposed an improved Kalman filter strategy, but the extraction of positive and negative sequence signals is too dependent on its covariance matrix and its parameters, which has great limitations. The second-order generalized integrator (SOGI) has the function of frequency selection and is also used as a phase detector in PLL [24]. With the advantages of frequency adaptation, small amount of calculation and strong immunity, it can achieve synchronous phase locking under the condition of voltage imbalance and distortion. Therefore, in recent years, the research on second-order generalized integrators and similar structures has become a research hotspot [25], such as: PLL based on double second-order generalized integrators [26] (DSOGI-based PLL), PLL based on multiple generalized integrators [27] (Multiple SOGI-based PLL), PLL based on adaptive notch filter [28] (Adaptive notch filter-based PLL). However, these methods have the problems of complex structure and large amount of calculation.

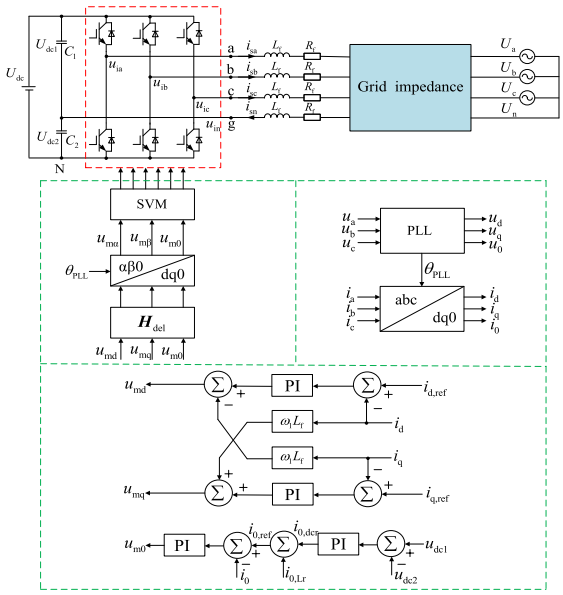

FIGURE 1. Control diagram of three-phase four-wire inverter connected to power grid.

In this paper, a phase-locked strategy based on complex filter matrix (CFM) is proposed. Based on the idea of Leon's positive and negative sequence component matrix operator, the first-order complex filter is introduced, and the orthogonal signal generator (OSG) is designed by matrix operation. The orthogonal signal generator has band-pass and low-pass characteristics for the original signal, and has the function of frequency selection and orthogonal signal extraction. Based on the orthogonal signal generator, a filter structure with positive and negative sequence cross feedback is designed to realize the positive and negative sequence extraction and decoupling of the original signal. The module is embedded in the phase detection link to realize the positive sequence phase locking strategy of the grid voltage fundamental wave. Through simulation and experimental verification, the proposed phase-locked method improves the phase margin of the three-phase four-wire grid-connected inverter system at low frequency, effectively suppresses the low-frequency oscillations of the grid-connected system under weak grid, and improves the reliability of the power system. Compared with the traditional phase-locked loop, the phase-locked loop can quickly and accurately obtain the fundamental voltage phase information in the input grid voltage signal under the grid distortion, and has a better dynamic response process.

II. LOW FREQUENCY OSCILLATION ANALYSIS OF GRID CONNECTION SYSTEM WITH THREE-PHASE FOUR-WIRE INVERTER

A. MAIN CIRCUIT OF GRID-CONNECTED SYSTEM

As shown in Fig.1, the equivalent control block diagram of the grid connection system of the three-phase four-wire inverter

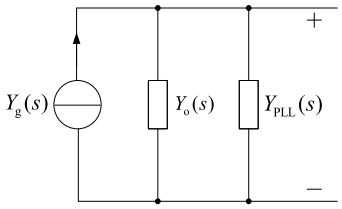

FIGURE 2. Impedance model of grid-connected inverter considering PLL effect.

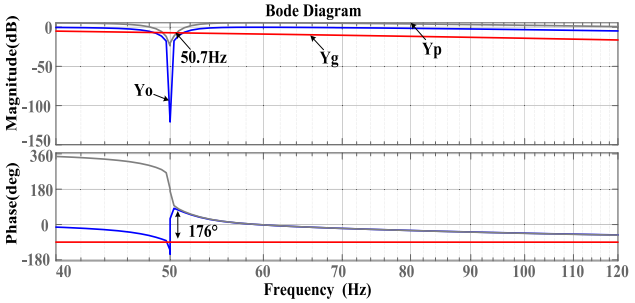

FIGURE 3. Bode diagram of output impedance of the three-phase four-wire inverter before and after PLL is considered in the inverter.

is clearly clarified, with the main circuit of the inverter and the grid connection control block diagram of the inverter. In terms of the main circuit of the three-phase four-wire inverter, u_{ia}, u_{ib}, u_{ic} and u_{in} represent the voltage of the four bridge arms of the inverter, i_{sa}, i_{sb}, i_{sc}, and i_{sn} represent the current of the four bridge arms, and U_a, U_b, and U_c represent the voltage of the grid connection Public Connection Point (PCC). In terms of the three-phase four-wire inverter control system, the controller mainly consists of grid connection phase current control, phase-locked loop, and conversion module. θ_{LL} is the phase angle in the Phase Locked Loop (PLL) module. In terms of the control block diagram, i_d, i_q, and i_0 represent the d, q, and 0 axis components of the grid current respectively; u_{md}, u_{mq}, and u_{m0} are the d, q, and 0 axis output values of the current controller respectively; the transfer matrix H_{del} represents the inverter control delay link.

B. LOW FREQUENCY OSCILLATION ANALYSIS OF GRID-CONNECTED SYSTEM

When analyzing the influence of the phase-locked loop on the three-phase four-wire inverter, the equivalent impedance of the phase-locked loop can be deemed as the external impedance of the inverter. As shown in Fig.2, the Norton's equivalent circuit model of the three-phase four-wire inverter system is clarified, where $Y_o(s)$ represents the output admittance without taking phase locking into consideration, and $Y_{PLL}(s)$ represents the additional admittance in the output impedance taking the influence of the phase-locked loop into consideration. Where, the positive sequence admittance of the inverter corresponding to paralleled $Y_o(s)$ and $Y_{PLL}(s)$ is expressed as $Y_p(s)$.

As shown in Fig. 3, the output impedance Bode plot of the three-phase four-wire inverter before and after the phase-locked loop is clarified. In this paper, the frequency scanning measurement software is Matlab2023a, and the hardware is the frequency scanning instrument GC-2/3/4GS8000. Without taking the influence of the phase-locked loop into consideration, the phase difference between the equivalent admittance $Y_g(s)$of the power grid and the output admittance $Y_o(s)$ of the three-phase four-wire inverter at the amplitude intersection point frequency is 150°, where the system is stable. On the contrary, taking the additional admittance of the phase-locked loop into consideration, the negative attenuation introduced by the additional admittance of the phase-locked loop causes the intersection frequency to shift towards the low frequency. The phase difference between $Y_o(s)$ and $Y_p(s)$ at the intersection frequency of 50.7Hz is 176° which is close to 180°. In accordance with the impedance stability theory, we know that the system stability margin is low, and there is a risk of low frequency oscillation instability in the interaction system between the inverter and the power grid.

Therefore, the additional attenuation introduced by the pase-locked loop will damage the original low frequency stability of the three-phase four-wire inverter system.

III. OSG DESIGN BASED ON COMPLEX FILTER MATRIX

A. PRINCIPLE OF FIRST-ORDER COMPLEX FILTERS

To reduce the influence of fundamental negative sequence voltage components and harmonics on SRF-PLL, it is necessary to extract the fundamental positive sequence components before coordinate transformation. To achieve the separation of positive and negative sequence signals, the paper proposes a first-order complex filter with polarity selectivity, as shown in Formula (1), where the first is a positive sequence filter, the second is a negative sequence filter, and the third is a zero sequence filter.

$$\begin{cases} F^{+}(s) = \dfrac{\omega_c}{s - j\hat{\omega} + \omega_c} \\ F^{-}(s) = \dfrac{\omega_c}{s + j\hat{\omega} + \omega_c} \\ F^{0}(s) = \dfrac{\omega_c}{s + \omega_c} \end{cases} \tag{1}$$

where, $\hat{\omega}$ is the fundamental angular frequency signal of the grid voltage, and ωc is the cut-off angular frequency signal of the first-order positive and negative zero sequence filters. Through calculation, the data shows that the positive sequence filter has an amplitude of 1 and a phase shift of 0 at the $\hat{\omega}$ frequency; with the signal frequency moving away from $\hat{\omega}$, the amplitude of the signal rapidly damps. Similarly, for negative sequence filters, the fundamental negative sequence component in the power grid voltage signal can pass through without attenuation or zero phase shift, while the fundamental positive sequence signal only shows small attenuation and is not completely filtered out. Therefore, when singly applying this first-order complex filter, we can achieve zero phase shift through the corresponding voltage component without attenuation and suppress harmonic components, but fail to achieve decoupling and separation of positive and negative sequence components. The paper intends to combine these two filters to

achieve fundamental voltage positive and negative sequence separation and harmonic suppression.

B. DESIGN OF FIRST-ORDER COMPLEX FILTERS

When the three-phase voltage is unbalanced, and in accordance with the Lyon method, the positive sequence, negative sequence, and zero sequence components of the fundamental voltage can be calculated as follows, after converting the voltage vector from the abc coordinate system to $\alpha\beta\gamma$ coordinate system.

$$\begin{cases} \boldsymbol{U}^{+}_{\alpha\beta\gamma} = \dfrac{1}{2}\begin{bmatrix} 1 & -q & 0 \\ q & 1 & 0 \\ 0 & 0 & 0 \end{bmatrix}\begin{bmatrix} u_\alpha \\ u_\beta \\ u_\gamma \end{bmatrix} \\ \boldsymbol{U}^{-}_{\alpha\beta\gamma} = \dfrac{1}{2}\cdot\begin{bmatrix} 1 & q & 0 \\ -q & 1 & 0 \\ 0 & 0 & 0 \end{bmatrix}\cdot\begin{bmatrix} u_\alpha \\ u_\beta \\ u_\gamma \end{bmatrix} \\ \boldsymbol{U}^{0}_{\alpha\beta\gamma} = \begin{bmatrix} 0 & 0 & 0 \\ 0 & 0 & 0 \\ 0 & 0 & 1 \end{bmatrix}\cdot\begin{bmatrix} u_\alpha \\ u_\beta \\ u_\gamma \end{bmatrix} \end{cases} \tag{2}$$

where,

$$\boldsymbol{T}_{\alpha\beta\gamma} = \sqrt{\frac{2}{3}}\begin{bmatrix} 1 & -\dfrac{1}{2} & -\dfrac{1}{2} \\ 0 & \dfrac{\sqrt{3}}{2} & -\dfrac{\sqrt{3}}{2} \\ \sqrt{\dfrac{1}{2}} & \sqrt{\dfrac{1}{2}} & \sqrt{\dfrac{1}{2}} \end{bmatrix}$$

is Clarke transformation matrix;

$q = e^{-\mathrm{j}(\pi/2)}$ is the phase shift operator for two-phase sinusoidal signals, representing the phase lag of $\pi/2$ in the time domain.

As shown in Formula (2), the decoupling of positive and negative sequence signals can be realized through linear operation by leading and lagging the signal in the time domain. However, influenced by the inability to obtain leading signals, it is unavailable to process them in the frequency domain temporarily. Therefore, the paper intended to apply the same phase shift operator structure to extract positive and negative sequence signals in the frequency domain.

Based on the above relationship, the paper intended to select a singular matrix to form an operational matrix, as shown in (3).

$$\begin{cases} \boldsymbol{P}^{+} = \dfrac{1}{2}\begin{bmatrix} 1 & \mathrm{j} & 0 \\ -\mathrm{j} & 1 & 0 \\ 0 & 0 & 0 \end{bmatrix} \\ \boldsymbol{P}^{-} = \dfrac{1}{2}\begin{bmatrix} 1 & -\mathrm{j} & 0 \\ \mathrm{j} & 1 & 0 \\ 0 & 0 & 0 \end{bmatrix} \\ \boldsymbol{P}^{0} = \begin{bmatrix} 0 & 0 & 0 \\ 0 & 0 & 0 \\ 0 & 0 & 1 \end{bmatrix} \end{cases} \tag{3}$$

To eliminate the influence of harmonic components on the separation of positive and negative sequences during the decoupling process, the paper combined first-order complex filters and an operational matrix, and constructed a complex filter matrix in the complex frequency domain:

$$\begin{cases} \boldsymbol{P}^{+}\boldsymbol{\Gamma}^{+} = \begin{bmatrix} F^{+}(s) & \mathrm{j}F^{+}(s) & 0 \\ -\mathrm{j}F^{+}(s) & F^{+}(s) & 0 \\ 0 & 0 & 0 \end{bmatrix} \\ \boldsymbol{P}^{-}\boldsymbol{\Gamma}^{-} = \begin{bmatrix} F^{-}(s) & -\mathrm{j}F^{-}(s) & 0 \\ \mathrm{j}F^{-}(s) & F^{-}(s) & 0 \\ 0 & 0 & 0 \end{bmatrix} \\ \boldsymbol{P}^{0}\boldsymbol{\Gamma}^{0} = \begin{bmatrix} 0 & 0 & 0 \\ 0 & 0 & 0 \\ 0 & 0 & F^{0}(s) \end{bmatrix} \end{cases} \tag{4}$$

To separate signal transformation and positive and negative sequence, the paper designed an Orthogonal Signal Generator (OSG) signal processing module based on the Complex Filter Matrix (CFM), and defined the input signals x1, x2, and x3, and output signals x1, x2, and x3. Through selecting the linear combined complex matrices, the relationship between the input and output signals of the signal processing module can be represented as (5), as shown at the bottom of the next page, where, $k_c = \omega_c/\hat{\omega}$.

In accordance with the definition of OSG, the function of the module is to filter a single input and obtain its orthogonal signal. Therefore, ordering $x_2 = x_2'$ and $x_3 = x_1 - x_1'$, that is, introducing output x_2' as feedback to the input, and applying self-feedback as input signal processing. The above process can be represented by the filter transmission matrix signal processing unit, as shown in Fig. 4.

Through further organizing Formula (5), the following signal conversion process can be established.

$$\begin{bmatrix} x_1'(s) \\ x_2'(s) \\ x_3'(s) \end{bmatrix} = \begin{bmatrix} \dfrac{\omega_c(s+\omega_c)}{s^2+2\omega_c s+\omega_c^2+\hat{\omega}^2} & \dfrac{-\omega_c\hat{\omega}}{s^2+2\omega_c s+\omega_c^2+\hat{\omega}^2} & 0 \\ \dfrac{\omega_c\hat{\omega}}{s^2+2\omega_c s+\omega_c^2+\hat{\omega}^2} & \dfrac{\omega_c(s+\omega_c)}{s^2+2\omega_c s+\omega_c^2+\hat{\omega}^2} & 0 \\ 0 & 0 & \dfrac{\omega_c^2}{\hat{\omega}(s+\omega_c)} \end{bmatrix} \times \begin{bmatrix} x_1(s) \\ x_2'(s) \\ x_1(s)-x_1'(s) \end{bmatrix} \tag{6}$$

As shown in Formula (6), the imaginary part of the designed orthogonal signal generator module is eliminated after feedback and calculation, and a simpler form is obtained, achieving efficient calculation.

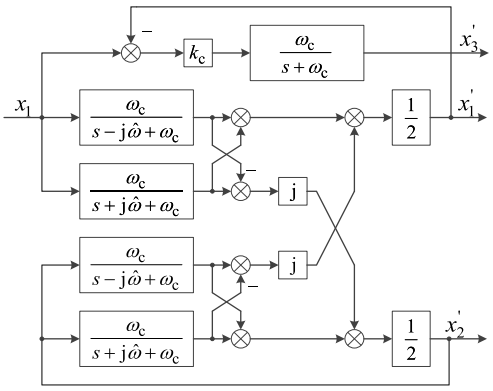

FIGURE 4. Filter transfer matrix signal processing module.

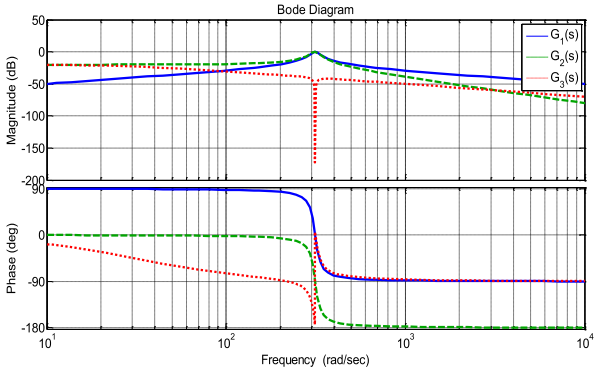

FIGURE 5. Bode diagram of filter transfer matrix module.

C. ANALYSIS OF CFM-OSG WORKING PRINCIPLE

Through analyzing Formula (6), the transfer function of the single input three output system can be expressed as:

$$\begin{cases} G_1(s) = \dfrac{x_1'(s)}{x_1(s)} = \dfrac{\omega_c s}{s^2 + \omega_c s + \hat{\omega}^2} \\ G_2(s) = \dfrac{x_2'(s)}{x_1(s)} = \dfrac{\omega_c \hat{\omega}}{s^2 + \omega_c s + \hat{\omega}^2} \\ G_3(s) = \dfrac{x_3'(s)}{x_1(s)} = \dfrac{\omega_c^2(s^2 + \hat{\omega}^2)}{\hat{\omega}(s+\omega_c)(s^2 + \omega_c s + \hat{\omega}^2)} \end{cases} \tag{7}$$

Selecting a fundamental frequency of 50Hz and a low-pass filter cutoff frequency of 5Hz, the Bode plots of the filter transmission matrix module can be obtained, as shown in Fig. 5.

Observing the Bode plot, $G_1(s)$ is a band pass filter with a central angular frequency of $\hat{\omega}$. If the angular frequency of the input signal is $\hat{\omega}$, the output signal has no amplitude attenuation and no phase shift; if the input signal is from another frequency band, the output signal will be attenuated in varied degrees. $G_2(s)$ is a low pass filter with a center angle frequency of $\hat{\omega}$, where the amplitude attenuation of the input signal at the center angle frequency is 0 and the output phase is reduced by 90 ° than that of the input signal. $G_3(s)$ is a band stop filter with a center angular frequency of $\hat{\omega}$. As shown in the Bode plot, the amplitude and phase characteristics of low frequency range are consistent, showing that the amplitude of the input signal at the center frequency is attenuated, while the input signal greater than the center frequency will be subjected to strong attenuation.

Integrating the above analysis and Formula (7), we can know that the signal can be subtracted, that is $x_2' - x_3'$, so as to achieve the goal to attenuate the orthogonal signals in the intermediate and low frequency bands. Based on the phase relationship between the transfer functions $G_1(s)$ and $G_2(s) - G_3(s)$ the paper obtained, the signal generator unit can be reshaped into a single input dual output system, with the transfer function expression as follows:

$$\begin{cases} G_{OSG1}(s) = G_1(s) = \dfrac{\omega_c s}{s^2 + \omega_c s + \hat{\omega}^2} \\ G_{OSG2}(s) = G_2(s) - G_3(s) = \dfrac{\omega_c s(\hat{\omega}^2 - \omega_c s)}{\hat{\omega}(s+\omega_c)(s^2 + \omega_c s + \hat{\omega}^2)} \end{cases} \tag{8}$$

In the two-phase stationary coordination system, the zero sequence component is basically no relationship to the phase-locked loop. Therefore, the zero-sequence component can be ignored in the phase-locked loop operation, and the grid voltage can be approximately deemed as positive and negative sequence components. Therefore, the improved phase-locked loop proposed in Formula (8) by the paper can be used for positive and negative sequence separation decoupling and harmonic suppression of three-phase four-wire grid connection inverters. Therefore, the improved phase-locked loop based on matrix transformation proposed by paper is shown in Fig. 6.

$$\begin{aligned} \begin{bmatrix} x_1'(s) \\ x_2'(s) \\ x_3'(s) \end{bmatrix} &= \boldsymbol{P}^+\boldsymbol{\Gamma}^+ \begin{bmatrix} x_1(s) \\ x_2(s) \\ x_3(s) \end{bmatrix} + \boldsymbol{P}^-\boldsymbol{\Gamma}^- \begin{bmatrix} x_1(s) \\ x_2(s) \\ x_3(s) \end{bmatrix} + k_c\boldsymbol{P}^0\boldsymbol{\Gamma}^0 \begin{bmatrix} x_1(s) \\ x_2(s) \\ x_3(s) \end{bmatrix} \\ &= (\boldsymbol{P}^+\boldsymbol{\Gamma}^+ + \boldsymbol{P}^-\boldsymbol{\Gamma}^- + k_c\boldsymbol{P}^0\boldsymbol{\Gamma}^0) \begin{bmatrix} x_1(s) & x_2(s) & x_3(s) \end{bmatrix}^{\mathrm{T}} \\ &= \frac{1}{2} \begin{bmatrix} \dfrac{\omega_c}{s-j\hat{\omega}+\omega_c} + \dfrac{\omega_c}{s+j\hat{\omega}+\omega_c} & j\dfrac{\omega_c}{s-j\hat{\omega}+\omega_c} - j\dfrac{\omega_c}{s+j\hat{\omega}+\omega_c} & 0 \\ -j\dfrac{\omega_c}{s-j\hat{\omega}+\omega_c} + j\dfrac{\omega_c}{s+j\hat{\omega}+\omega_c} & \dfrac{\omega_c}{s-j\hat{\omega}+\omega_c} + \dfrac{\omega_c}{s+j\hat{\omega}+\omega_c} & 0 \\ 0 & 0 & \dfrac{2k_c\omega_c}{s+\omega_c} \end{bmatrix} \begin{bmatrix} x_1(s) \\ x_2(s) \\ x_3(s) \end{bmatrix} \end{aligned} \tag{5}$$

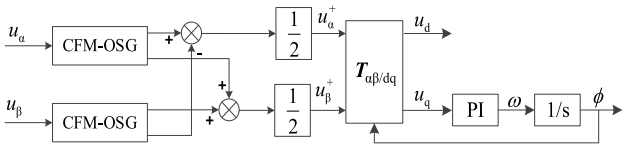

FIGURE 6. Improved phase-locked loop based on CFM-OSG transformation.

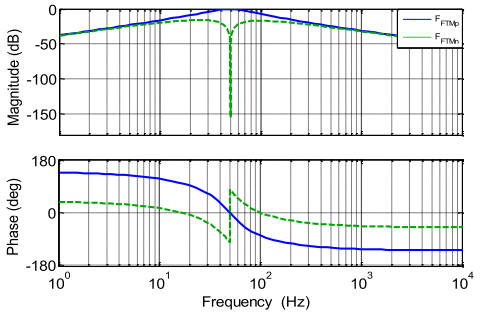

FIGURE 7. Bode diagram of filter transfer matrix.

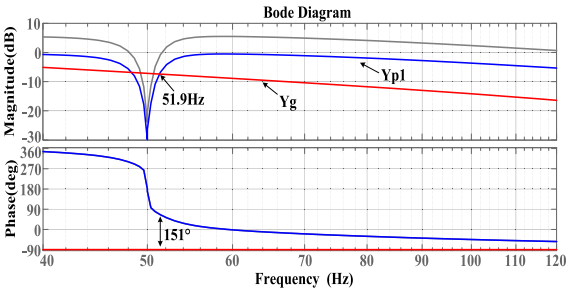

FIGURE 8. Output admittance of three-phase four-wire inverter based on matrix transformation proposed in this paper.

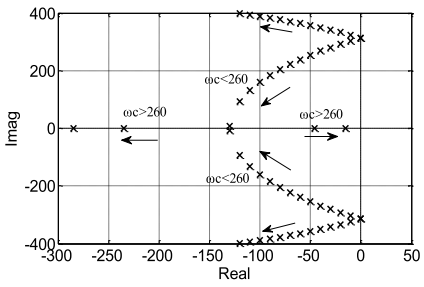

FIGURE 9. Root locus diagram of inverter system with different control parameters ω_c.

IV. OSG CHARACTERISTICS ANALYSIS BASED ON COMPLEX FILTER MATRIX

A. IMPROVED PHASE-LOCKED LOOP ADMITTANCE MODEL

As shown in Formula (8), the transmission matrix of voltage positive sequence and negative sequence filters in the frequency domain can be derived and represented as follows (9), as shown at the bottom of the next page:

Therefore, the Bode plot of filter transfer matrix can be clarified, as shown in Fig. 7.

Through analyzing Fig.7, we can know that, when extracting the positive and negative sequence components of the power grid voltage, the designed complex filter matrix unit exhibits a band pass characteristic without phase shift for the positive sequence component of the input voltage, and a zero phase shift band stop notch characteristic for the negative sequence component of the voltage. Where, the closed-loop transfer function of the improved phase-locked loop can be expressed as:

$$G'_{\mathrm{PLL}}(s) = \begin{cases} G_{\mathrm{filter\_p}}(s)(s)G_{\mathrm{PLL}}(s), & f = f_{\mathrm{p}} \\ G_{\mathrm{filter\_n}}(s)(s)G_{\mathrm{PLL}}(s), & f = f_{\mathrm{n}} \end{cases} \tag{10}$$

B. ADMITTANCE CHARACTERISTICS ANALYSIS OF IMPROVED PHASE-LOCKED LOOP

Through organizing the positive and negative sequence transfer functions of Formula (10) into additional admittance forms and introducing them into the three-phase four-wire inverter, the output admittance Bode plot is shown in Fig. 8. Compared with the traditional SRF-PLL phase-locked loop, when the proposed CFM-OSG phase-locked loop is used, the frequency of the admittance intersection between the inverter and the power grid shifts from 50.7Hz to 51.9Hz, and the phase difference at the frequency of the intersection between the inverter and the power grid changes from 176° to 151°. The stability margin of the low frequency system is further improved.

Considering the steady-state time, $\hat{\omega} = 314$rad/s is selected, according to the Formula (8), the root locus of the system is shown in Fig.9, while the parameter ω_c is different. As shown in the Fig.9, when the parameter ω_c changes from 0 to 260, the root trajectory of the system characteristic function moves away from the imaginary axis, the dynamic response speed and stability margin of the system increase; when ω_c changes from 260 to 314, the dominant feature roots move towards the imaginary axis direction, the system response speed and stability margin decreases. Based on the frequency characteristics analysis of the OSG module, it can be concluded that the larger the ω_c, the better the frequency selection characteristics.

In conclusion, introducing a complex filter transmission matrix orthogonal signal generator in the phase-locked loop is equivalent to connecting a unit with band pass filtering characteristics in the forward channel of the phase-locked loop, achieving accurate extraction of input voltage positive and negative sequence signals, which not only reduces the impact of negative sequence voltage on the output signal of the phase-locked loop, but also improves the accuracy of the extraction and separation of positive sequence voltage in the phase-locked loop. Standing from the perspective of impedance analysis, it is equivalent to series correction of the three-wire four-wire inverter grid-connected system, which makes the frequency of the intersection point between the inverter and the power grid to move towards the high frequency, and the phase difference between the two at the low frequency further away from 180°, which effectively reduces the risk of low frequency oscillation instability introduced

TABLE 1. Parameters of the experimental platform of the proposed inverter.

Parameter	Value
Output power P_o(kW)	30
Line voltage U_{Line} (V)	380
DC bus voltage U_{dc} (V)	700
Output frequency f_o (Hz)	50
Switching frequency f_{sw} (kHz)	10
Power factor cosφ	0.8
Filter inductor L_f(mH)	1.7
L_f equivalent resistance R_f(mΩ)	2.5
DC-link capacitor C_1, C_2(μF)	1200

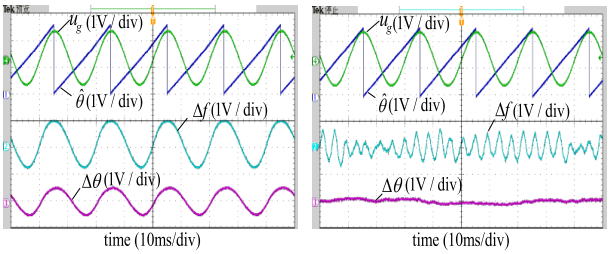

(a) Traditional SRF-PLL (b) Novel CFM-OSG

FIGURE 10. Experimental waveforms when the grid voltage contains DC offset.

by the phase-locked loop in the three-phase four-wire inverter.

V. EXPERIMENT VERIFICATION

To verify the feasibility of applying CFM-OSG phase-locked loop to suppress low frequency oscillations in three-phase four-wire inverters, the paper established the prototype of three-phase four-wire inverters and conducted experiments for verification, where the core chip of the main control unit of the prototype adopted TMS320F28335 of TI. To simulate a weak current network, a reactor was connected in series at the output end of the power grid. The main parameters of the model are listed in Table.1.

A. COMPARATIVE ANALYSIS OF PHASE LOCKING ACCURACY

As shown in Fig. 10-12, the experimental comparison waveform between traditional SRF-PLL and improved SRF-PLL is clarified, and the experimental results of phase locking accuracy is shown in Table.2.

Through analyzing Fig. 10-12 and Table 1, we can know that when there is a DC offset, harmonic component, and frequency fluctuation in the grid side voltage, the traditional phase-locked loop has a higher phase-locked error. While, the

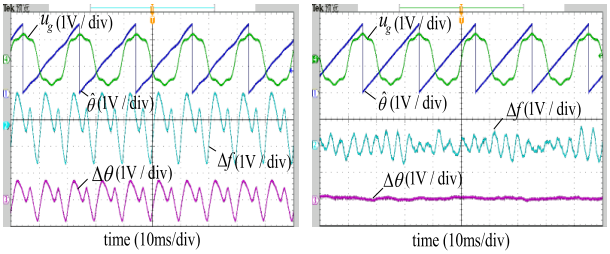

(a) Traditional SRF-PLL (b) Novel CFM-OSG

FIGURE 11. Experimental waveforms when grid voltage is distorted with harmonics.

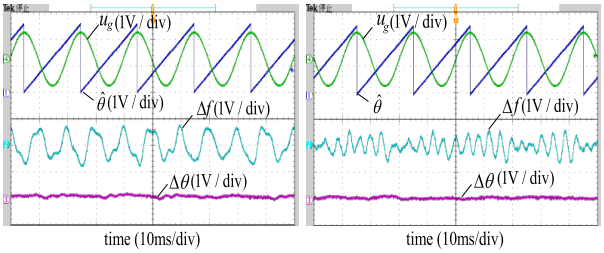

(a) Traditional SRF-PLL (b) Novel CFM-OSG

FIGURE 12. Experimental waveforms when grid-frequency fluctuation.

TABLE 2. Experimental results of phase-looking precision.

power grid condition	frequency error (Hz)		phase angle error (°)	
	conventional method	improved method	conventional method	improved method
DC biasing	1.4	0.15	8.9	0.82
harmonics	1.2	0.09	7.5	0.78
frequency	2.1	0.05	13.4	0.70

improved phase-locked loop designed by the paper has strong adaptability, with lower output error of the phase-locked loop.

B. COMPARATIVE ANALYSIS OF LOW FREQUENCY OSCILLATION SUPPRESSION

To verify the influence of traditional SRF-PLL on three-phase four-wire inverters, the paper set the phase-locked loop control parameters to $k_{p\_PLL} = 5$ and $k_{i\_PLL} = 100$, and set the grid impedance to 2mH. Meanwhile, to verify the dynamic and steady-state performance of the inverter system, two three-phase four-wire inverters were connected during the experiment for verification. As shown in Fig. 13, it illustrates the waveform of the grid connection current of the inverter when using a traditional SRF-PLL phase-locked loop. Through observation, we can know that the system can operate stably when one inverter is connected to the

$$\begin{cases} G_{\text{filter\_p}}(s) = \dfrac{G_{\text{OSG1}}(s) + \text{j}G_{\text{OSG2}}(s)}{2} = \dfrac{\omega_c\hat{\omega}s(s+\omega_c) + \text{j}\omega_c s(\hat{\omega}^2 - \omega_c s)}{2\hat{\omega}(s+\omega_c)(s^2+\omega_c s+\hat{\omega}^2)}, & f = f_p \\ G_{\text{filter\_n}}(s) = \dfrac{G_{\text{OSG1}}(s) - \text{j}G_{\text{OSG2}}(s)}{2} = \dfrac{\omega_c\hat{\omega}s(s+\omega_c) - \text{j}\omega_c s(\hat{\omega}^2 - \omega_c s)}{2\hat{\omega}(s+\omega_c)(s^2+\omega_c s+\hat{\omega}^2)}, & f = f_n \end{cases} \tag{9}$$

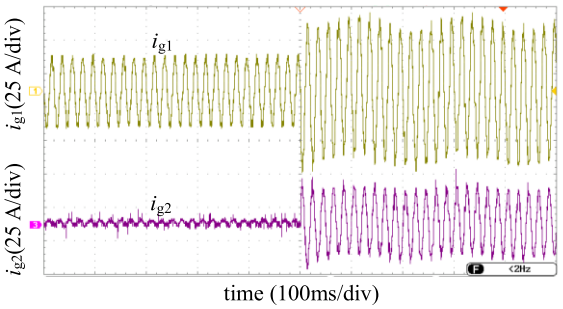

FIGURE 13. Experimental waveform of inverter grid current based on SRF-PLL.

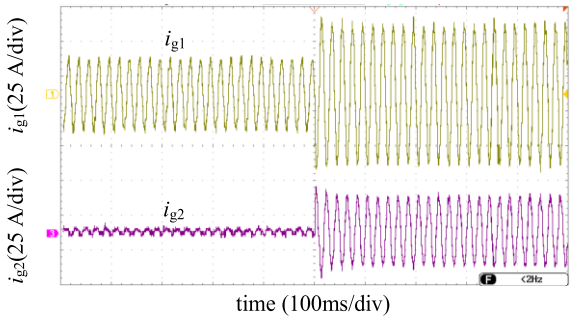

FIGURE 14. Experimental waveform of grid current of inverter based on CFM-OSG.

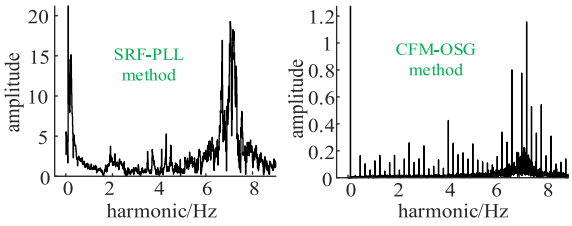

FIGURE 15. FFT analysis of three-phase four-wire inverter grid-connected system.

grid, while low frequency oscillation occurs when the second inverter is put into operation.

The three-phase four-wire inverter adopts the output current of the CFM-OSG phase-locked loop, as shown in Fig. 14. Through observation, we can know that when one inverter is connected to the grid, the system can operate stably, and when the second inverter is put into operation, the system can still operate stably and the output power quality is high.

C. COMPARATIVE ANALYSIS OF TOTAL HARMONIC DISTORTION

The frequency spectrum analysis of voltage harmonic components, amplitudes, and contents in the grid connected system under different operating conditions is shown in Fig. 15. When the grid connected system uses traditional SRF-PLL, the harmonic components are mainly 6-8Hz low frequency harmonics; when applying CFM-OSG proposed by the paper, low frequency harmonics of 6-8Hz can be effectively suppressed.

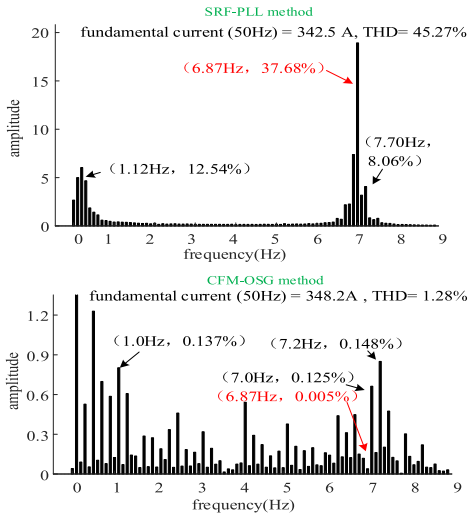

FIGURE 16. FFT comparison of three-phase four-wire inverter grid-connected system.

The details of Fig.15 are shown in Fig.16. The above figure shows a grid connected system that uses a traditional SRF-PLL phase-locked loop to generate low frequency oscillations. At the oscillations point (6.87Hz), the harmonic amplitude is 45.27% of the fundamental current; the following figure shows a grid connected system using a CFM-OSG phase-locked loop, demonstrating the effective suppression of low frequency oscillations in the grid connected system. The total harmonic distortion rate of the grid connected current has been reduced from 45.27% to 1.28%, meeting the requirement of no more than 5% THD for grid connected current in GB/T 37408-2019 standard. This strongly proves the effectiveness of the low frequency oscillations mechanism analysis and the new CFM-OSG phase-locked loop in suppressing low-frequency oscillation.

VI. CONCLUSION

This paper proposes a suppression strategy for low-frequency oscillations of three-phase four-wire inverter grid-connected system caused by phase-locked loop in weak grid environment. Firstly, the mechanism of low frequency oscillation caused by phase-locked loop in weak grid is analyzed. Secondly, an improved phase-locked loop (CFM-OSG) based on matrix transformation is proposed, which makes the intersection frequency of inverter and grid admittance move to high frequency, and the stability margin of three-phase four-wire inverter system at low frequency under weak grid is effectively improved. Finally, the experimental results show that the proposed method can effectively suppress the low-frequency oscillation of the three-phase four-wire inverter system.

However, when designing the control algorithm, the influence of grid impedance on the system and its stability is not considered. The next step is to analyze the grid and load as a whole to verify the effectiveness of CFM-OSG in suppressing low-frequency oscillation under weak grid conditions.

REFERENCES

[1] Z. Zhang, P. Wang, P. Jiang, F. Gao, L. Fu, and Z. Liu, "Robust control method of grid-connected inverters with enhanced current quality while connected to a weak power grid," *IEEE Trans. Power Electron.*, vol. 37, no. 6, pp. 7263–7274, Jun. 2022.

[2] J. Luo, H. Zhang, S. Zhang, W. Wu, H. Ouyang, and Y. Chen, "Modeling and characteristic analysis of sequential impedance of three-phase off-grid inverter under unbalanced load," *Power System Protection Control*, vol. 48, no. 12, pp. 33–40, 2020.

[3] M. Cheah-Mane, L. Sainz, J. Liang, N. Jenkins, and C. E. Ugalde-Loo, "Criterion for the electrical resonance stability of offshore wind power plants connected through HVDC links," *IEEE Trans. Power Syst.*, vol. 32, no. 6, pp. 4579–4589, Nov. 2017.

[4] X. Xie, H. Liu, J. He, C. Zhang, and Y. Qiao, "Mechanism and characteristics of subsynchronous oscillation caused by the interaction between full-converter wind turbines and AC systems," *Proc. CSEE*, vol. 36, no. 9, pp. 2366–2372, 2016.

[5] S. Hasanzadeh, H. Shojaeian, M. M. Mohsenzadeh, E. Heydarian-Forushani, H. H. Alhelou, and P. Siano, "Power quality enhancement of the distribution network by multilevel STATCOM-compensated based on improved one-cycle controller," *IEEE Access*, vol. 10, pp. 50578–50588, 2022.

[6] A. F. Cupertino, W. C. S. Amorim, H. A. Pereira, S. I. S. Junior, S. K. Chaudhary, and R. Teodorescu, "High performance simulation models for ES-STATCOM based on modular multilevel converters," *IEEE Trans. Energy Convers.*, vol. 35, no. 1, pp. 474–483, Mar. 2020.

[7] H. Haitao, H. Zhengyou, and Q. Chenghao, "Modal analysis based research on dynamic harmonic resonance of all-parallel autotransformer traction supply network," *Power Syst. Technol.*, vol. 36, no. 1, pp. 163–169, 2012.

[8] D. Song, X. Yang, Q. Ding, and Q. Wang, "A survey analysis on low frequency oscillation in large-scale interconnected power grid and its control methods," *Power Syst. Technol.*, vol. 35, no. 10, pp. 22–28, 2011.

[9] H. Xin, Z. Li, W. Dong, L. Zhang, Z. Wang, and J. Zhao, "Generalized-impedance and stability criterion for grid-connected converters," *Proc. CSEE*, vol. 37, no. 5, pp. 1277–1292, 2017.

[10] W. Chen, F. Blaabjerg, N. Zhu, M. Chen, and D. Xu, "Doubly fed induction generator wind turbine systems subject to recurring symmetrical grid faults," *IEEE Trans. Power Electron.*, vol. 31, no. 2, pp. 1143–1160, Feb. 2016.

[11] Z. P. Wei, T. Zheng, and J. Li, "Short circuit current analysis of DFIG with crowbar under unsymmetrical grid fault," in *Proc. 2nd IET Renew. Power Gener. Conf. (RPG)*, Sep. 2013, pp. 1–4.

[12] G. Pannell, D. J. Atkinson, and B. Zahawi, "Analytical study of grid-fault response of wind turbine doubly fed induction generator," *IEEE Trans. Energy Convers.*, vol. 25, no. 4, pp. 1081–1091, Dec. 2010.

[13] H. Xu, J. Hu, and Y. He, "Operation of wind-turbine-driven DFIG systems under distorted grid voltage conditions: Analysis and experimental validations," *IEEE Trans. Power Electron.*, vol. 27, no. 5, pp. 2354–2366, May 2012.

[14] A. M. A. Haidar, K. M. Muttaqi, and M. T. Hagh, "A coordinated control approach for DC link and rotor crowbars to improve fault ride-through of DFIG based wind turbines," *IEEE Trans. Ind. Appl.*, vol. 53, no. 4, pp. 4073–4086, May 2017.

[15] G. Pannell, D. J. Atkinson, and B. Zahawi, "Minimum-threshold crowbar for a fault-ride-through grid-code-compliant DFIG wind turbine," *IEEE Trans. Energy Convers.*, vol. 25, no. 3, pp. 750–759, Sep. 2010.

[16] W. Hui and W. Mingli, "Simulation analysis on low-frequency oscillation in traction power supply system and its suppression method," *Power Syst. Technol.*, vol. 39, no. 4, pp. 1088–1095, 2015.

[17] X. Yusheng, "Comprehensive defense evolved from accidental failure to power disaster-warning of '8/14' blackout in North America," *Autom. Electr. Power Syst.*, vol. 27, no. 18, pp. 1–5, 2003.

[18] Z. Liang, M. Xiao, K. Zhang, J. Zhou, and J. Wu, "Discussion on control strategy of low frequency oscillation in southern power grid," *Automat. Electr. Power Syst.*, vol. 35, no. 16, pp. 54–58, 2011.

[19] T. Bi, Y. Kong, S. Xiao, P. Zhang, and T. Zhang, "Review of sub-synchronous oscillation with large-scale wind power transmission," *J. Electr. Power Sci. Technol.*, vol. 27, no. 1, pp. 10–15, 2012.

[20] R. Zhang, M. Cardinal, P. Szczesny, and M. Dame, "A grid simulator with control of single-phase power converters in D-Q rotating frame," in *Proc. IEEE 33rd Annu. IEEE Power Electron. Spec. Conf.*, Jun. 2002, pp. 1431–1436.

[21] M. Bongiorno, J. Svensson, and A. Sannino, "Effect of sampling frequency and harmonics on delay-based phase-sequence estimation method," *IEEE Trans. Power Del.*, vol. 23, no. 3, pp. 1664–1672, Jul. 2008.

[22] Z. Yao, "Fundamental phasor calculation with short delay," *IEEE Trans. Power Del.*, vol. 23, no. 3, pp. 1280–1287, Jul. 2008.

[23] K. De Brabandere, T. Loix, K. Engelen, B. Bolsens, J. Van den Keybus, J. Driesen, and R. Belmans, "Design and operation of a phase-locked loop with Kalman estimator-based filter for single-phase applications," in *Proc. IEEE IECON*, Apr. 2006, pp. 525–530.

[24] P. Rodríguez, A. Luna, R. S. Muñoz-Aguilar, I. Etxeberria-Otadui, R. Teodorescu, and F. Blaabjerg, "A stationary reference frame grid synchronization system for three-phase grid-connected power converters under adverse grid conditions," *IEEE Trans. Power Electron.*, vol. 27, no. 1, pp. 99–112, Jan. 2012.

[25] S. Golestan, M. Monfared, F. D. Freijedo, and J. M. Guerrero, "Dynamics assessment of advanced single-phase PLL structures," *IEEE Trans. Ind. Electron.*, vol. 60, no. 6, pp. 2167–2177, Jun. 2013.

[26] J. A. Suul, A. Luna, P. Rodriguez, and T. Undeland, "Voltage-sensor-less synchronization to unbalanced grids by frequency-adaptive virtual flux estimation," *IEEE Trans. Ind. Electron.*, vol. 59, no. 7, pp. 2910–2923, Jul. 2012.

[27] P. Rodriguez, A. Luna, M. Ciobotaru, R. Teodorescu, and F. Blaabjerg, "Advanced grid synchronization system for power converters under unbalanced and distorted operating conditions," in *Proc. 32nd Annu. Conf. IEEE Ind. Electron.*, Nov. 2006, pp. 5173–5178.

[28] P. Rodríguez, A. Luna, I. Candela, R. Mujal, R. Teodorescu, and F. Blaabjerg, "Multiresonant frequency-locked loop for grid synchronization of power converters under distorted grid conditions," *IEEE Trans. Ind. Electron.*, vol. 58, no. 1, pp. 127–138, Jan. 2011.

GUOXUAN CUI was born in Beijing, China, in 2002. He is currently a student in electrical engineering and automation with the School of Mechanical and Electrical Engineering, China University of Mining and Technology, Beijing, and is expected to graduate in June 2025. His primary research interest lies in power systems and automation.

YANWEN WANG was born in Tangshan, China, in 1962. He is currently a Professor with the School of Mechanical and Electrical Engineering, China University of Mining and Technology, Beijing. He majored in electrical engineering and automation. He has printed more than 30 papers (SCI). His primary research interests are power systems and automation.

LIYA LIU was born in Hengshui, Hebei, in 1990. She graduated in in applied chemistry from North China Electric Power University in 2016. She is currently working with Beijing Bowang Technology Company Ltd. Her main research interests are renewable energy and microgrid research.